

# Lens distortion in optically coupled digital x-ray imaging

Hong Liu,<sup>a)</sup> Hangyi Jiang, and Laurie L. Fajardo

Department of Radiology and Biomedical Engineering, Johns Hopkins University, Baltimore, Maryland 21205

Andrew Karellas

Department of Radiology, University of Massachusetts Medical Center

Wei R. Chen

Department of Physics and Engineering, University of Central Oklahoma

(Received 8 March 2000; accepted for publication 10 March 2000)

The objectives of this research are to analyze geometrical distortions introduced by relay lenses in optically coupled digital x-ray imaging systems and to introduce an algorithm to correct such distortions. *Methods:* The radial and tangential errors introduced by a relay lens in digital x-ray imaging were experimentally measured, using a lens-coupled CCD (charge coupled device) prototype. An algorithm was introduced to correct these distortions. Based on an x-ray image of a standard calibration grid, the algorithm first identified the location of the optical axis, then corrected the radial and tangential distortions using polynomial transformation technique. *Results:* Lens distortions were classified and both radial and tangential distortions introduced by lenses were corrected using polynomial transformation. For the specific lens-CCD prototype investigated, the mean positional error caused by the relay lens was reduced by the correction algorithm from about eight pixels (0.69 mm) to less than 1.8 pixels (0.15 mm). Our investigation also shows that the fourth order of polynomial for the correction algorithm provided the best correction result. *Conclusions:* Lens distortions should be considered in position-dependant, quantitative x-ray imaging and such distortions can be minimized in CCD x-ray imaging by appropriate algorithm, as demonstrated in this paper. © 2000 American Association of Physicists in Medicine. [S0094-2405(00)03705-6]

Key words: lens distortion, optically coupled x-ray imaging system, camera calibration

## I. INTRODUCTION

Both fiber optically coupled and lens-coupled CCD x-ray imaging systems have been used in digital mammography and digital radiography.<sup>1-3</sup> The cascaded imaging chain consists of a scintillator, an optical component (either a relay lens or a spatial coherent fiber bundle), and an electronic imager, such as a CCD imager.<sup>4-6</sup> Obviously, the optical properties of the lens, or the fiber, can affect the quality of the x-ray imaging significantly. In our previous communications, the characteristics of optical fiber taper and its impact on image contrast were analyzed.<sup>7</sup> The impact of lens-coupling efficiency on signal-to-noise ratio was investigated.<sup>8</sup> This communication focuses on the geometrical distortions caused by relay lenses, since it is well known that aberrations, including geometrical distortions, do exist even with a well-designed and well-built lens. We will first introduce the origin of lens geometrical distortion. We will then take the lens-coupled CCD x-ray imaging system as an example to analyze the positional errors introduced by lens geometrical distortion. Finally, we will present an algorithm for correcting geometrical distortions caused by lens in digital x-ray imaging.

## II. GEOMETRICAL DISTORTIONS CAUSED BY LENS

As shown by Fig. 1, a relay lens used in an optically coupled CCD x-ray imaging system collects light from a

point on a scintillator, and focuses it onto a corresponding conjugate point on an electronic imager. Under the most practical conditions, the lens, same as all other optical components, is not able to form a perfect image due to the presence of aberrations. Lens aberrations include spherical aberration, coma, field curvature, astigmatism, axial color, lateral color, and distortion.<sup>9</sup> Most of these aberrations degrade the image quality by “blurring” the image.

Lens distortion is a unique aberration in that it does not degrade the quality of the image in terms of sharpness and focus. Rather, it affects the shape of the image, causing it to depart from a true-scaled duplication of the original object. For instance, if one acquires the image of a square grid as shown in Fig. 2(a), the recorded image can be affected by pincushion distortion, as shown in Fig. 2(b), and affected by barrel distortion, as shown in Fig. 2(c). Pincushion is an outward displacement of a given image point from its desired location on a mean image plane: Its magnitude increases, in the simplest cases, as the field angle of the optical system increases. The field angle  $\alpha$  is defined in Fig. 1. On the other hand, barrel distortion is an inward displacement, and its magnitude also increases with the field angle, but with a different orientation [see Fig. 2(c)]. The distortions demonstrated in Fig. 2 are only radial distortions, which for a purely rotational system cause the actual image point to be displaced radially in the image plane, independent of the azimuth in the field.

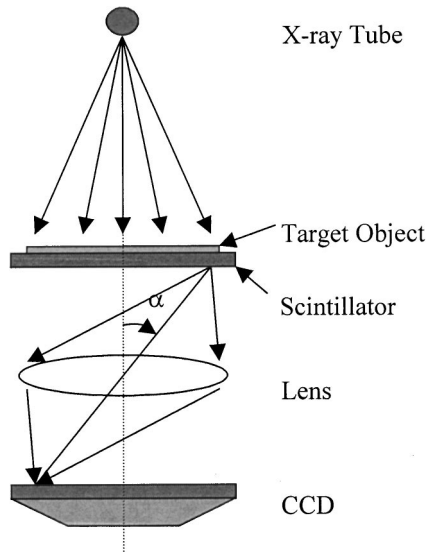


FIG. 1. A schematic of a lens-coupled CCD digital x-ray imaging system. The field angle  $\alpha$  is defined as the angle formed by the optical axis (dotted line) and the principal ray through the center of the lens connecting the two conjugate points.

In principle, a lens is a rotationally symmetric system. In practice, no ideal lenses can be made. Small errors retained in the alignment and centering of a multielement optical system lead to tangential displacement of image point; the magnitude of such distortion depends on both the azimuth and the off-axis position of the field. Figure 3 shows an example of the tangential distortion. One of the effects of tangential distortion is that a straight line passing through the center of the field may be recorded as a weakly curved line.

Lens aberrations cannot be avoided completely in optical design; however, they can be minimized. Optical designers evaluate the potential contribution of each aberration to the final system performance and adjust the configuration of the optical assembly to achieve satisfactory performance for each application. For instance, an optical designer usually balances the outward and inward displacements to minimize geometrical distortions. The designer, however, has to “trade-off” many factors, such as cost and size, against technical parameters required by specific applications. With exception of certain custom built systems, distortion errors in the range of 1–3 percent may be present in commercially available relay lenses, when these lenses are used in the imaging system.

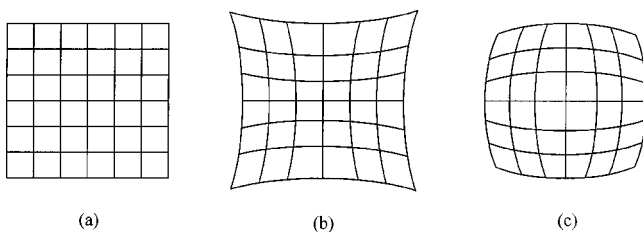


FIG. 2. Illustration of geometrical distortions introduced by lens. (a) A checkerboardlike grid without distortion; (b) Pincushion distortion; (c) Barrel distortion.

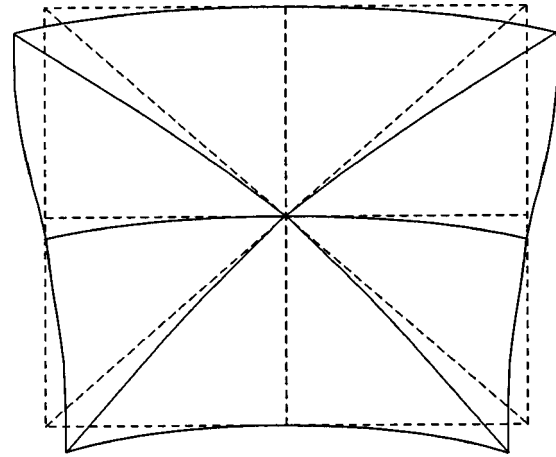


FIG. 3. Illustration of tangential distortion: A straight line passing through the center (optical axis) of the field is recorded as a weakly curved line. In this schematic, the dashed lines show the undistorted geometrical pattern and the solid lines represent the distorted pattern.

Due to the presence of the residual distortion, the local scale on an image produced by a lens-coupled digital x-ray imaging system may vary both radially and tangentially at a given image position from the mean value.

In many diagnostic-imaging applications, such as routing gastrointestinal fluoroscopy, the presence of geometrical distortions is often unnoticed by the image readers (its effect on the diagnostic quality is up to discussion). The presence of geometrical distortions is, however, of great importance in position-dependent, quantitative imaging, such as in cardiac catheter placement, neurological embolization procedures, and in image guided biopsy. For instance, the errors introduced by both radial and tangential distortions reduce the positional accuracy of a lens-coupled CCD stereotactic system.

### III. POSITIONAL ERROR INTRODUCED BY LENS

To investigate the geometrical distortion introduced by lenses in digital x-ray imaging, a lens-coupled CCD prototype was used.<sup>3</sup> The system, consisting of a scintillating screen ( $\text{Gd}_2\text{O}_2\text{S:Tb}$ ), a relay lens and a CCD camera, is attached to a clinical x-ray machine. The camera employs a mechanical shutter. An optical hood was used to shield the CCD sensor from ambient light. The CCD array size is  $1024 \times 1024$  pixels, and  $0.024 \text{ mm} \times 0.024 \text{ mm}$  per pixel. The camera was operated under a temperature of  $-25^\circ \text{C}$  to reduce thermal electron noise. The low temperature was achieved with a compact thermoelectric cooler. The operation of the system is described as follows: (1) During x-ray exposure, the x-ray beam passing through the testing target is attenuated and interacts with the scintillating screen. (2) The x-ray photons are then converted into a large number of visible light photons. (3) The relay lens projects the optical scene from the scintillating screen to the photosensitive surface of the CCD camera. (4) The CCD pixel array samples the information and creates a digital image. In our experi-

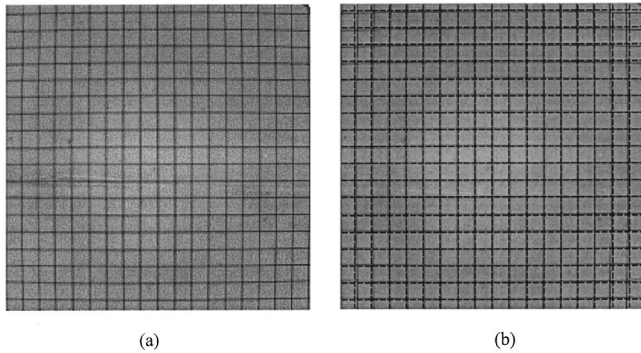


FIG. 4. Digital x-ray images showing the effect of lens distortion. (a) An x-ray image of a checker board like grid, acquired using a prototype lens-coupled CCD x-ray imaging system, (b) a standard map of the grid (dashed lines), properly scaled, was artificially overlaid on the distorted x-ray image, to demonstrate the geometrical distortion.

ment, this operation was controlled by a computer. The x-ray energy and exposure used in the experiments were 30 kVp and 32 mAs, respectively.

A commercial Nikon lens, F/1.2, 50 mm focal length, equipped with a close-up (Nikon Close-up #2) lens was used as the relay lens to project the optical image from the scintillating screen to the CCD imager. The relay lens is working at a 3.6:1 demagnification ratio, thus making an object of one millimeter in length occupy  $\sim 11.6$  pixels in digital image. During experiments, a checkerboard-like grid made by copper wires was imaged by the prototype system. To minimize the effect of x-ray focal spot on image quality and geometrical shape, the copper wires were kept directly against the scintillator (no air gap between the testing target and the x-ray detector), and the distance from the x-ray focal spot to the scintillator was kept at 650 mm. The diameter of the copper wires was 0.17 mm and the spacing between the copper wires (center to center) was 5 mm.

An x-ray image of the calibration grid acquired by our imaging system is shown in Fig. 4(a). In Fig. 4(b), a map of the grid (dashed lines), properly scaled, is artificially overlaid over the acquired image, to demonstrate the geometrical distortion. At locations near the center of the image (near the optical axis of the lens), the standard map overlaps with the x-ray image almost perfectly. At locations toward the edges of the image, the displacement between the map and the x-ray image becomes clearly noticeable. Apparently, this specific lens used in this prototype introduced a significant barrel distortion.

To quantitatively measure positional errors introduced by lens distortions in digital x-ray imaging, positional displacement of the grid image from its true location was calculated for all the feature points (intersections of the grid wires). In

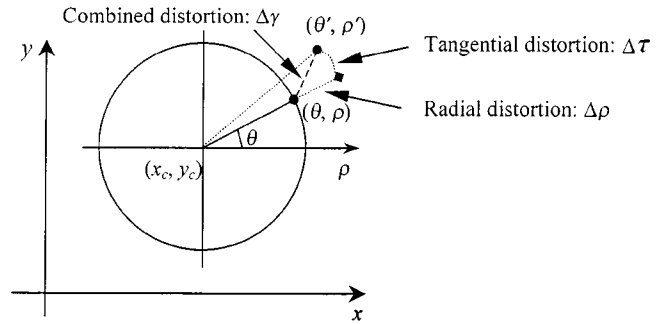


FIG. 5. Illustration of the coordinate system to characterize lens distortions. The optical center  $(x_c, y_c)$  is served as the origin of polar domain. The base axis of the polar system is parallel to the  $x$  axis of Cartesian system. The distorted and undistorted points are denoted as  $(\rho, \theta)$  and  $(\rho', \theta')$ , respectively. The radial distortion,  $\Delta\rho$ , tangential distortion,  $\Delta\tau$ , and combined distortion,  $\Delta\gamma$ , are also illustrated in this figure.

Table I, radial distortion errors, and total distortion errors (combined radial and tangential errors) are listed as functions of the field angle of the optical system. The radial distortion error,  $\Delta\rho$ , and the total distortion error,  $\Delta\gamma$ , are illustrated in Fig. 5 in a polar coordinate.

As shown in Table I, the positional displacement of an object imaged by such a lens-coupled digital x-ray imaging system can be, in the most severe cases, more than nine pixels away from its true location within a field angle of  $30^\circ$ . Considering the fact that the CCD imager used in the prototype has only  $1024 \times 1024$  pixels, the positional error introduced by the lens distortion cannot be neglected in any position-dependent, quantitative x-ray imaging.

#### IV. AN ALGORITHM FOR LENS DISTORTION CORRECTION

Digital image processing techniques can be used to correct geometrical distortions introduced by optical and optoelectronic components.<sup>10-12</sup> In our study, a correction algorithm was introduced to minimize the lens distortion. The algorithm was derived based on the nature of the lens distortion.

After a digital image of a standard grid is acquired by the imaging system, the algorithm operates as follows:

- (1) Localize the intersections of the wires of the grid (feature points);
- (2) Create an ideal map of the grid;
- (3) Identify the optical center of the lens;
- (4) Perform polynomial-transformation to correct distortions.

TABLE I. Positional errors introduced by relay lens versus field angle of the optical system.

Field angle $\alpha$ (degree)	3.6	8.6	13.0	17.4	22.1	26.2	30.0
Radial distortion $\Delta\rho$ (pixel)	1.26	2.28	3.25	4.30	5.43	6.94	7.42
Combined distortion $\Delta\gamma$ (pixel)	2.39	3.16	4.15	5.19	6.61	8.04	9.71
Combined distortion $\Delta\gamma$ (mm)	0.20	0.27	0.36	0.45	0.57	0.69	0.84

These procedures are discussed in detail in the succeeding text.

**A. Localizing feature points**

A semiautomatic procedure was developed to localize the positions of the feature points (wire intersections of the grid). The first step of this procedure was to manually locate two adjacent feature points, which served as the starting points of the semiautomatic procedure.<sup>13</sup> Centered at each of the starting points, a local window was set up (40×40 pixels rectangle in our experiment). A connected region was determined that contained *m* adjacent pixels (*m*=8 in our experiment) with the lowest gray levels inside the window. This region could be named as a valley region. Because of the superposition of the two wires, the x-ray attenuation at each intersection of the grid (feature point) was higher. Therefore, feature points showed minimum pixel value in the image. It is reasonable to assume that the feature point was located inside the valley region. The reason for chosen a connected region instead of a pixel is to improve the algorithm’s robustness for the unavoidable imaging noise, and to improve the accuracy of the locations of the feature points. The exact location of the feature point (*x<sub>a</sub>*, *y<sub>a</sub>*) was defined as the gravity center of the valley region

$$\begin{aligned} x_a &= \frac{1}{m} \sum_{i=1}^m x_i f(x_i, y_i) \\ y_a &= \frac{1}{m} \sum_{i=1}^m y_i f(x_i, y_i), \end{aligned} \tag{1}$$

where *f(x<sub>i</sub>, y<sub>i</sub>)* was the gray level at point (*x<sub>i</sub>*, *y<sub>i</sub>*) in the valley region.<sup>14,15</sup> Using Eq. (1), the first two feature points, their starting points being manually located, can be determined in sub-pixel accuracy.

The algorithm could identify the next starting point according to the distance between two known feature points along the extension (or perpendicular) line between them, since the calibration image was a checkerboardlike grid. One by one, the remaining feature points were determined by using this method.

**B. Creating the ideal map of the grid**

The ideal map of the grid was created to serve as the standard pattern for image correction. In Ref. 16, Shah and Aggarwal acquired an ideal image by another lens that introduced minimal distortion. If the polynomial warping method was employed, the grid target could be used as an undistorted ideal grid itself.<sup>16</sup> Here, a method was employed to create an ideal map of the grid from the actual distorted grid image using the following mechanism.

The grid pattern consisted of two sets of parallel straight lines intersecting at a right angle. One set of parallel lines can be described by the equation:

$$y_i = kx + ib \quad (i = \dots -1, 0, 1, \dots), \tag{2}$$

where the parameters *k* and *b* are the slope and the *y*-separation of the lines, respectively. It is reasonable to as-

sume that the lens distortion is negligible near the center of the image. Thus, the parameters *k* and *b* can be estimated using feature points in the center region of the actual grid image. In our experiment, with the whole image size of 1024×1024 pixels, a 200×200-pixel sub-image was taken around the image center for the purpose of the parameter calculation. This sub-image covers four pairs of straight lines. Each line equation was initially determined using two calculated feature points as described above. Then in the perpendicular direction along this line, the points with a local minimum gray level were localized. Using the least mean-square fitting method, the parameters of the line equation could be determined precisely with these local minimum gray level points. The calculated grid map of the center region was then extended to the whole image, thereby creating the entire calculated grid map. However, the map was roughly positioned with respect to the geometrical center of the x-ray image array. The last step of this procedure was, therefore, to shift the calculated grid map slightly to achieve the best alignment with the actual grid image by minimizing the following criterion function

$$F = \sum_i [(x_{gi} - x_{ai})^2 + (y_{gi} - y_{ai})^2], \tag{3}$$

where (*x<sub>g</sub>*, *y<sub>g</sub>*) and (*x<sub>a</sub>*, *y<sub>a</sub>*) are the feature points corresponding to the calculated grid map and actual grid image, respectively. The subscript *i* indicates the *i*th feature point, and the summation in Eq. (3) is over all feature points of the x-ray image.

**C. Identifying the optical center of the lens**

Normally, the lens distortion is mainly in radial direction, which causes an inward or outward displacement of a given image point from its true location. This type of distortion is strictly symmetric about the optical axis.<sup>17-19</sup> With this property, a method was developed to localize the optical center (optical axis).

Let (*x<sub>c</sub>*, *y<sub>c</sub>*) denote the optical center, the radial distortion at any feature point (*x<sub>ai</sub>*, *y<sub>ai</sub>*) in the actual image can be calculated by:

$$\begin{aligned} d(x_{ai}, y_{ai}) &= \sqrt{(x_{ai} - x_c)^2 + (y_{ai} - y_c)^2} \\ &\quad - \sqrt{(x_{gi} - x_c)^2 + (y_{gi} - y_c)^2}, \end{aligned} \tag{4}$$

where, (*x<sub>gi</sub>*, *y<sub>gi</sub>*) is the corresponding feature point to the (*x<sub>ai</sub>*, *y<sub>ai</sub>*) in the calculated ideal grid map.

For feature point (*x<sub>ai</sub>*, *y<sub>ai</sub>*), its symmetric location about the optical center (*x<sub>c</sub>*, *y<sub>c</sub>*) is given by (2*x<sub>c</sub>* - *x<sub>ai</sub>*, 2*y<sub>c</sub>* - *y<sub>ai</sub>*). Therefore, the asymmetry of the radial distortion to (*x<sub>c</sub>*, *y<sub>c</sub>*) can be characterized by a function

$$J(x_c, y_c) = \sum_i [d(x_{ai}, y_{ai}) - d(2x_c - x_{ai}, 2y_c - y_{ai})], \tag{5}$$

where the subscript *i* indicates the *i*th feature point. The summation is over all feature points of the x-ray image. The optical center is such a point that the asymmetry of the distortion is at a minimum level. Therefore, the problem of

searching the exact location of the optical center is equivalent to an optimization procedure in which the center position  $(x_c, y_c)$  is to be determined in order to minimize the object function  $J$  in Eq. (5).

To perform such an optimization procedure, the following steps were adopted:

- (1) First, select the center of the digital image as the initial location for the optical center.
- (2) Search for  $x_c$ , by minimizing the object function  $J$  in Eq. (5) with  $y_c$  fixed.
- (3) Then, with a fixed  $x_c$  determined in step 2, search for  $y_c$  by minimizing  $J$ .
- (4) Repeat steps 2 and 3 until the location of the optical center is stabilized within a reasonable tolerance (0.2 pixels in our experiment).

It should be noted that for a feature point  $(x_a, y_a)$ , its symmetric point  $(2x_c - x_a, 2y_c - y_a)$  about the center  $(x_c, y_c)$  may be falling between the known grid wire intersections. In such a situation, a two-dimensional interpolation was implemented according to its neighbors to seek an estimate of its radial distortion. Bilinear interpolation was used in our method.<sup>20</sup>

**D. Performing polynomial-transform to correct distortion**

Polynomial transformation is a common method used to correct the distortions.<sup>21-23</sup> Since a combination of radial distortion and tangential distortion was seen in the image, in our experiment two sets of polynomials were needed. One was used to correct the radius as measured from the optical center, and the other was used to correct the polar angle as measured from the base axis of the polar system. As shown in Fig. 5, the distorted image of a feature point is denoted as polar coordinate  $(\rho, \theta)$ , and the distortion-free image of the point is denoted as  $(\rho', \theta')$ . The radial position of each pixel and the tangential offset component were corrected by applying two set of  $N$ -order polynomials:

$$\begin{aligned} \theta' &= a_1\theta + a_2\theta^2 + a_3\theta^3 + a_4\theta^4 + \dots, \\ \rho' &= b_1\rho + b_2\rho^2 + b_3\rho^3 + b_4\rho^4 + \dots, \end{aligned} \tag{6}$$

where,  $a_i$  and  $b_i$  are the distortion coefficients. The above equations hold for all feature points of the image. Because the number of feature points generally exceeded the number of polynomial coefficients,  $a_i$  and  $b_i$  were solved by least-squares fitting which minimized the mean-square error between the calculated positions from Eq. (6) and the undistorted positions in ideal grid map. The two sets of coefficient  $a_i$  and  $b_i$  can be used for the corrections of all image signals.

**V. RESULTS AND DISCUSSIONS**

**A. Effectiveness of the algorithm**

This algorithm was applied to the images acquired by our prototype lens-coupled digital x-ray imaging system. The corrected images in Fig. 6 showed a significant distortion

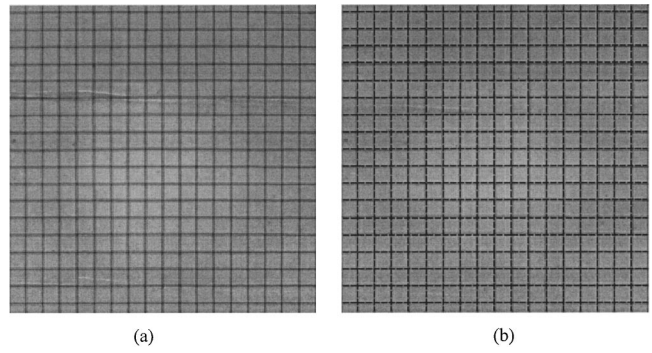


Fig. 6. Digital x-ray images showing the effect of distortion. (a) The corrected result of the grid image by fourth-order polynomials (see the image of the grid before the correction in Fig. 4). The mean residual error was reduced from 8.04 pixel to 1.78 pixel. (b) A standard grid map (dashed lines) was overlaid on the corrected grid image to show the minimized geometrical distortion. Compare with Fig. 4 to see the effect of the correction.

reduction when compared with the uncorrected images in Fig. 4.

To quantitatively measure the effectiveness of the correction algorithm, the absolute mean residual error (positional displacement of the grid image from its true location) was calculated for all of the intersections of the grid wires. The mean residual error before correction was 8.04 pixels and after corrections 1.78 pixels. In Fig. 7, the mean values of the radial distortion error,  $\Delta\rho$ , before and after correction are plotted as function of the field angle  $\alpha$  of the optical system (refer to Fig. 1 for the definition of  $\alpha$ ). In Fig. 8, the mean values of the combined distortion error,  $\Delta\gamma$ , before and after correction, are also plotted versus the field angle  $\alpha$  (refer to Fig. 5 for illustration of  $\Delta\rho$  and  $\Delta\gamma$ ).

Clearly, the polynomial algorithm effectively corrected the lens distortion in digital x-ray imaging.

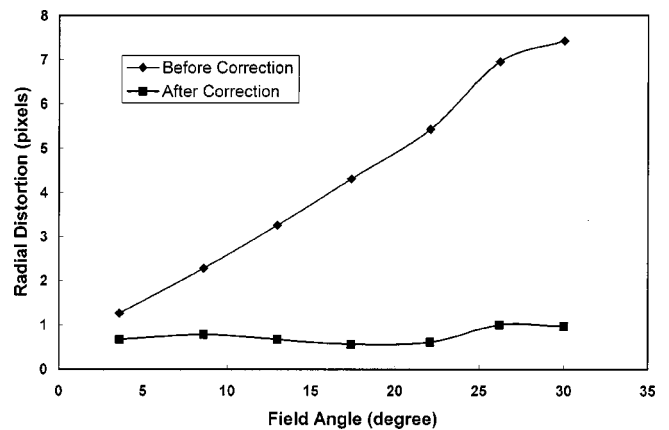


Fig. 7. The mean radial distortion errors before and after correction as a function of field angle of the optical system. Before the correction, the error ranges from 1.26 pixels (0.109 mm) to 7.42 pixels (0.64 mm). After correction, the mean error ranges from 0.56 pixels (0.05 mm) to 1.00 pixels (0.086 mm).

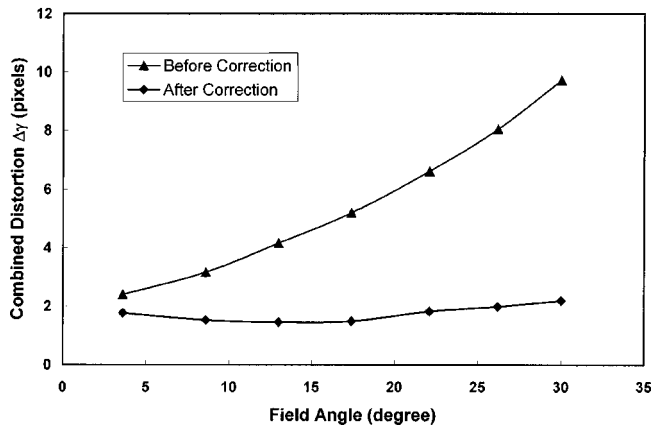


FIG. 8. The combined distortion errors  $\Delta\gamma$  with respect to field angle before and after correction (refer to Fig. 5 for the definition of  $\Delta\gamma$ ). Before the correction, the error ranges from 2.39 pixels (0.206 mm) to 9.71 pixels (0.84 mm). After correction, the error ranges from 1.45 pixels (0.125 mm) to 2.18 pixels (0.19 mm).

## B. Order of polynomials and its impact on distortion correction

As described previously, two sets of  $N$ -order polynomials were used in correcting both radial and tangential distortions. It is important to select a proper order of  $N$  to achieve optimized result. Theoretically, higher-order polynomial leads to less residual error. However, higher-order polynomials can also cause oscillation and make the mathematical solutions unstable. In our experiments, the effect of different orders of the polynomials on lens distortion correction was tested by generating sets of coefficients for orders:  $N=2, 3, 4, 5, 6$ . The mean residual errors after correction for different  $N$  values are listed in Table II. The results showed that the image correction improved as the order of the polynomial increased up to four. However, the correction effect decreased with higher-order polynomials.

In addition to the possible oscillation, another reason for lack of improvement was that it could lead to some extra round-off errors when the higher order polynomial transformation was performed. For the investigations using our imaging system, the optimal order of polynomials appeared to be four. The corresponding polynomial coefficients  $a_i$  and  $b_i$  are listed in Table III.

## VI. CONCLUSION

Optical coupling is an important link in various digital x-ray imaging systems. The optical properties of the components, either a lens, a fiber bundle or other optoelectronic device will affect the quality of clinical procedures significantly. There is no ideal optical component or optoelectronic

TABLE II. The mean residual errors of corrected image using polynomial transformation of different orders.

Polynomial order ( $N$ )	2	3	4	5	6
Mean residual error (Pixel)	2.14	2.02	1.78	3.94	4.77
Mean residual error (mm)	0.18	0.17	0.15	0.34	0.41

TABLE III. The polynomial coefficients used for correcting lens distortions ( $N=4$ ).

For radial Distortion	$a_1$	$a_2$	$a_3$	$a_4$
	1.008	$2.836 \times 10^{-5}$	$-1.634 \times 10^{-7}$	$1.091 \times 10^{-10}$
For tangential Distortion	$b_1$	$b_2$	$b_3$	$b_4$
	1.003	$-2.293 \times 10^{-4}$	$-4.751 \times 10^{-4}$	$3.074 \times 10^{-5}$

device that can relay an image without degrading its quality or distorting its shape. One could, however, balance the design trade-offs of the selected components according to the specific clinical applications.

Arguably, optical lens still is the most conventional and widely used imaging component. In comparison with many other optical techniques, lenses have many advantages, such as (1) cost effectiveness: It may be expensive to build just one or two custom lenses, but in mass production, lenses can be made at very low cost; (2) flexibility: Even with a simple relay lens, the parameters such as magnification, aperture, field of coverage, and depth of focus are adjustable; (3) image quality: A well-designed lens offers much higher spatial resolution than many other optical components or optoelectronic devices. For most commercial and custom lenses, aberrations are selectively minimized according to the specific applications. However, residual aberrations, including geometrical distortions do exist even with a well-designed and well-built lens. Although these residual distortions are usually small in terms of absolute or relative errors, they will reduce, for instance, the positional accuracy of image guided procedures.

The distortion introduced by relay lenses, however, can be minimized with digital image processing techniques. In fact, it is easier to correct distortions introduced by lenses than that by many other types of imaging components, since lens distortion is primarily radial and tangential dependant.<sup>24-27</sup> In other words, lens distortion may be ‘‘mapped’’ with a set of mathematical formulas and compensated accordingly using appropriate algorithms, as demonstrated in this paper.

We have shown that based on the nature and the classifications of lens distortion, the coefficients of the polynomial in the correction algorithm can be determined to minimize both radial and tangential distortions. For the specific imaging system investigated, the fourth order polynomials provided the best correction results. The low order polynomials were not sufficient for modeling the lens distortion, and the higher order polynomials tended to introduce oscillation that makes the algorithm unstable.

Overall, our analysis suggests that lens distortion should be considered in developing optically coupled digital x-ray imaging systems for position-dependant, quantitative x-ray imaging, and that residual geometrical distortions could be minimized effectively using digital image processing techniques. The advantages of using lens to relay images from scintillating screen to electronic imager are cost effectiveness, flexibility and image quality.

## ACKNOWLEDGMENTS

This work was supported in part by a NIH-NCI grant (Grant No. CA 70209) (P.I.: H Liu) and by a U.S. Army breast cancer research Grant No. DAMD 17-97-1-7138 (P.I.: H Liu).

- <sup>a)</sup> Author to whom correspondence should be addressed. Telephone: (410) 614-9291; Fax: (410) 614-7760. Electronic mail: hliu@jhim.edu
- <sup>1</sup> A. Karellas, L. Harris, H. Liu, M. Davis, and C. D'Orsi, "Charge-Coupled Device detector: Performance considerations and potential for mammographic imaging," *Med. Phys.* **19**, 1015–1023 (1992).
- <sup>2</sup> H. Liu, J. Xu, G. Halama, and J. McAdoo, "Digital fluoroscopy using an optically coupled CCD: Preliminary investigations," *SPIE Proceedings* **2976**, 256–261 (1997).
- <sup>3</sup> A. Jalink, J. McAdoo, G. Halama, and H. Liu, "CCD-mosaic technique for large field digital mammography," *IEEE Trans. Med. Imaging* **15**, 260–267 (1996).
- <sup>4</sup> H. Liu, L. L. Fajardo, J. R. Barrett, and R. A. Baxter, "Contrast-detail detectability analysis: comparison of a digital spot mammography system and an analog screen-film mammography system," *Acad. Radiol.* **4**, 197–203 (1997).
- <sup>5</sup> H. Liu, L. L. Fajardo, and B. Penny, "Signal-to-noise ratio, noise power spectrum and detective quantum efficiency analysis of optically coupled CCD mammography imaging systems," *Acad. Radiol.* **3**, 799–805 (1996).
- <sup>6</sup> H. Liu, A. Karellas, S. Moore, and L. Harris, "Lesion detectability considerations for an optically coupled CCD x-ray imaging system," *IEEE Trans. Nucl. Sci.* **41**, 1506–1509 (1994).
- <sup>7</sup> H. Liu, A. Karellas, L. Harris, and C. D'Orsi, "Optical properties of fiber tapers and their impact on the performance of a fiber optically coupled CCD x-ray imaging system," *SPIE Proceedings* **1894**, 136–147 (1993).
- <sup>8</sup> H. Liu, A. Karellas, and L. Harris, "Methods to calculate lens coupling efficiency in an optically coupled CCD x-ray imaging system," *Med. Phys.* **21**, 1193–1195 (1994).
- <sup>9</sup> B. H. Walker, "Primary lens aberrations," in *Optical engineering fundamentals* (SPIE Optical Engineering Press, Bellingham, Washington, 1998), pp. 129–148.
- <sup>10</sup> J. M. Boone, J. A. Seibert, W. A. Barrett, and E. A. Blood, "Analysis and correction of imperfections in the image-intensifier-tv-digitizer imaging chain," *Med. Phys.* **18**, 236–242 (1991).
- <sup>11</sup> R. Ning, J. K. Riek, and D. L. Conover, "An image intensifier based volume tomographic angiography imaging system: geometric distortion correction," *SPIE Proceedings* **2163**, 199–210 (1994).
- <sup>12</sup> B. Achueler and X. Hu, "Correction of image intensifier distortion for three-dimensional x-ray angiography," *SPIE Proceedings* **2432**, 272–279 (1996).
- <sup>13</sup> E. Gronenschild, "The accuracy and reproducibility of a global method to correct for geometric image distortion in the x-ray imaging chain," *Med. Phys.* **24**, 1875–1888 (1997).
- <sup>14</sup> E. L. Hall, *Computer Image Processing and Recognition* (Academic, New York, 1979), pp. 185–189.
- <sup>15</sup> K. R. Castleman, *Digital image Processing* (Prentice Hall, Upper Saddle River, New Jersey, 1996), pp. 120–127.
- <sup>16</sup> S. Shah and J. Aggarwal, "Intrinsic parameter calibration procedure for a (high distortion) fish-eye lens camera with distortion model and accuracy estimation," *Pattern Recogn.* **29**, 1775–1788 (1996).
- <sup>17</sup> Lasmea, "Camera Calibration from Spheres Images," *Proceedings of Computer Vision-ECCV'94*, Stockholm, Sweden (Springer-Verlag, Berlin, 1994), pp. 449–454.
- <sup>18</sup> D. C. Brown, "Close-range camera calibration," *Photogramm. Eng. Remote Sens.* **37**, 855–866 (1971).
- <sup>19</sup> *Manual of Photogrammetry*, 4th ed. (Amer. Soc. Photogrammetry, Falls Church, Virginia, 1980).
- <sup>20</sup> D. Ballard and C. Brown, *Computer Vision* (Prentice-Hall, Inc., Englewood Cliffs, New Jersey, 1982).
- <sup>21</sup> J. Weng, P. Cohen, and M. Hernion, "Camera calibration with distortion models and accuracy evaluation," *IEEE Trans. On PAMI-14*, No. **10**, 965–980 (1992).
- <sup>22</sup> Z. Jericevic, D. M. Benson, J. Bryan, and L. C. Smith, "Geometric correction of digital images using orthonormal decomposition," *J. Microsc.* **149**, Pt.3 233–245 (1988).
- <sup>23</sup> R. Fahrig, M. Moreau, and D. M. Holdsworth, "Three-dimensional computed tomographic reconstruction using a C-arm mount XR11: correction of image intensifier distortion," *Med. Phys.* **24**, 1097–1106 (1997).
- <sup>24</sup> D. C. Brown, "Decentering distortion of lenses," *Photogramm. Eng. Remote Sens.* **32**, 444–462 (1966).
- <sup>25</sup> R. Y. Tasi, "A versatile camera calibration technique for high-accuracy 3D machine vision metrology using off-the-shelf TV cameras and lenses," *IEEE Journal of Robotics and Automation* **3**, 323–344 (1987).
- <sup>26</sup> Y. Nomura, M. Sagara, H. Naruse, and A. Ide, "Simple calibration algorithm for high-distortion-lens camera," *IEEE Trans. On PAMI-14*, No. **11**, 1095–1099 (1992).
- <sup>27</sup> H. Bacakoglu and M. S. Kamel, "A three-step camera calibration method," *IEEE Trans. Instrum. and Measurement* **46**, 1165–1172 (1997).